Manipulability, Force, and Compliance Analysis for Planar Continuum Manipulators

Ian A. Gravagne and Ian D. Walker, *Senior Member, IEEE*

***Abstract*—Continuum manipulators, inspired by the natural capabilities of elephant trunks and octopus tentacles, may find niche applications in areas like human–robot interaction, multiarm manipulation, and unknown environment exploration. However, their true capabilities will remain largely inaccessible without proper analytical tools to evaluate their unique properties. Ellipsoids have long served as one of the foremost analytical tools available to the robotics researcher, and the purpose of this paper is to first formulate, and then to examine, three types of ellipsoids for continuum robots: manipulability, force, and compliance.**

***Index Terms*—Compliance, continuum robot, ellipsoid, hyperredundant, manipulability.**

I. Introduction

ANYONE who has observed an elephant for any length of time cannot help but watch in amazement at the creature's ability to control its environment through an appendage that contains no rigid parts whatsoever. It seems almost counterintuitive that an elephant's trunk, despite its flexibility, can in one moment lift huge weights (e.g., tree trunks) with apparent effortlessness, and in the next position itself with the necessary delicacy and precision to pick up a peanut. As with arms, legs, and hands, artificially constructed trunklike manipulators will likely never reach the zenith of complexity represented by the real thing. Nevertheless, some of the reproducible aspects and capabilities of trunks and tentacles could enrich the field of robotic manipulation in certain applications, like material transport from (or exploration of) unknown environments, and whole arm manipulation. Continuum manipulators' inherent passive compliance could also prove beneficial in human–robot interaction [18] and multiarm-cooperating manipulation by reducing reliance on complex force-feedback schemes that prevent the arms from fighting one another.

Trunk and tentaclelike devices belong to a category of manipulators termed continuum, for the lack of joints or rigid links. The alternate category, high-degree-of-freedom (HDOF) devices, might best be imagined as snake backbones, consisting of many joints connected by relatively short links.

Manuscript received June 29, 2001; revised January 23, 2002. This paper was recommended for publication by Associate Editor G. Chirikjian and Editor A. De Luca upon evaluation of the reviewers' comments. This work was supported in part by NASA under Grant NAG5-9785, in part by the NSF-EPSCOR program under Grant EPS-9630167, and in part by the South Carolina Space Consortium Graduate Fellowship Program. This paper was presented in part at the IEEE/RSJ Intelligent Robots and Systems Conference, Maui, HI, October 2001.

The authors are with the Department of Electrical and Computer Engineering, Clemson University, Clemson, SC 29634 USA (e-mail: igravag@ces.clemson.edu; ianw@ces.clemson.edu).

Publisher Item Identifier S 1042-296X(02)05180-7.

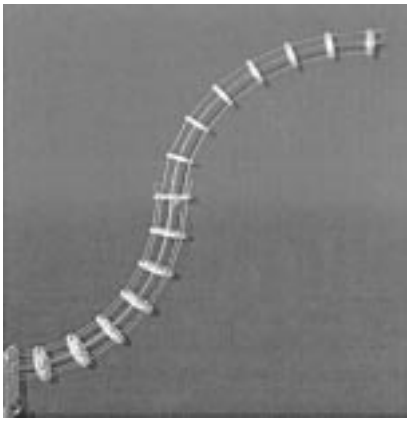

Fig. 1. Tentacle Manipulator.

In fact, the two classes, broadly categorized as hyperredundant, share many similarities, and a significant body of work exists attempting to describe the kinematics of HDOF devices with continuum models. It should be noted, however, that the dividing classifications mentioned above are somewhat imprecise, and the capabilities of a hyperredundant manipulator may be better characterized by noting the relation of its structure to its actuation scheme.

Several designs of elephant trunk or snakelike robots appear in [1], [6], [7], [13], [28], and [30]. Fig. 1 illustrates the Clemson Tentacle Manipulator. The Tentacle Manipulator is of very simple design [11], consisting of a highly elastic rod as its backbone, with antagonistic cable pairs periodically able to exert moments on the backbone to deform its shape. Although this is a truly continuous device, as a real tentacle is, it is only actuated with four degrees of freedom. Its underactuated backbone may adopt an infinite number of poses for a given actuator displacement, and endows it with the useful property of inherent passive compliance, which we will study shortly. On the other hand, Fig. 2 illustrates the Rice/Clemson Elephant's Trunk Manipulator [31]. Its backbone has 32 degrees of freedom, but only eight degrees are actuated; the other 24 are connected with a mesh of springs. Consequently, although it is actually an HDOF mechanism, it behaves with qualitative similarity to the Tentacle Manipulator, and in practice we often treat it as if it were a continuum device.

In contrast to the aforementioned manipulators, the HDOF devices analyzed in [6] and [20]–[22] are entirely controlled, with no underactuation at all. Their properties and capabilities differ substantially from the underactuated mechanisms. And, of course, there is a third option that does not yet exist (to our knowledge), a continuum manipulator continuously actu-

Fig. 2. Elephant's Trunk Manipulator.

ated. Interestingly, the significant differences between the various classes of manipulators do not render the models and mathematics derived for one class completely useless for another. To the contrary, unifying theories for kinematics, dynamics, control, and analysis seem to be developing, including standard robotic manipulators as a special case. Our purpose in this paper is to summarize a small cross section of that theory, concentrating on the expanded definitions of three new types of ellipsoids as they apply to underactuated continuum devices. After presenting some background work, we will define and derive the global and constrained manipulability and force ellipsoids for continuum robots, and then look at the passive compliance ellipsoid as well. Each case will conclude with simulated examples.

The ellipsoid provides one of the standard tools for studying a manipulator's characteristics, and a large volume of work discussing ellipsoids exists in the literature. A representative sample of the work appears in [2]–[4], [12], [17], [32], and [34]. Alternatives to ellipsoid analysis also exist, notably [23]. For background into the kinematics and path planning of continuum and hyperredundant robots, see [5], [6], [11], [14], [15], and [31]. The term "continuum" first appears in the survey paper [25]. The application of passive compliance and compliance ellipsoids to human–robot interaction appears in [18]. In this paper, we take an approach derived from the field of elastica mechanics. Details can be found in [9], [19], and [24]; furthermore, [7] is a significant work comparing HDOF and continuum methodologies.

II. Planar Continuum Kinematics

The continuum robots under consideration here are built upon one central, highly flexible, and elastic backbone. Modeling the reaction of an elastic member to a set of applied generalized forces is the *elastica* mechanics problem. In this paper, we make the assumption that the backbone never bends past the small-strain region, where an applied stress produces a strain that is recoverable and obeys an approximately linear stress–strain relationship. (It should be noted that small local strains integrated over a sufficiently long span can yield large displacements; small strain is frequently assumed in works such as [27].) This being the case, the nonlinearities in a continuum robot kinematic model exist for purely geometric reasons, yielding a great simplification. A thin elastic member, or beam, in two dimensions can undergo three basic types of deformations: bending, axial tension/compression, and shear (see [9]). Although this work can be adapted for extensible manipulators, long and thin backbones made from homogeneous materials will generally bend far more easily than they stretch and shear. Thus, we employ a nonextensible kinematic model that closely matches the characteristics of our prototype robot. If we define the independent parameterization variable $s \in [0, L]$ where L is the at-rest length of the beam, then we may specify the position of the beam $\underline{x}(s)$ and its cross-sectional angle $\theta(s)$ according to the governing field equations

$$EI\theta'' + \underline{x}'^T T \underline{f} + m = 0 \tag{1a}$$

$$\underline{x}' = \underline{q} \tag{1b}$$

where $(\cdot)' \triangleq d/ds$, $m(s)$ is a distributed moment applied to the beam, appearing later in (5), and EI is the bending stiffness. The other quantities are

$$T = \begin{bmatrix} 0 & 1 \\ -1 & 0 \end{bmatrix} \quad \underline{q} = \begin{bmatrix} c_\theta \\ s_\theta \end{bmatrix} \tag{2}$$

with $c_\theta = \cos(\theta)$ and $s_\theta = \sin(\theta)$; and $\underline{f}$ is a shear/axial force applied at the end-effector. (Underscores indicate vector quantities.) This formulation can be derived from that found in [27]. Note that we will use the identity

$$\underline{q}' = \theta' T^T \underline{q} \tag{3}$$

extensively throughout the paper. The boundary conditions for the solution of (1) are

$$\theta(0) = 0 \tag{4a}$$

$$\underline{x}(0) = \underline{0} \tag{4b}$$

$$EI\theta'(L) = 0. \tag{4c}$$

The first two conditions, the geometric conditions, reflect the fact that the backbone is clamped at the origin. The third is explained next.

The question arises, how should the model account for the application of moments by the actuators at points in the field, i.e., intermediate points along the backbone? Two possibilities exist. The most obvious is to treat each section of the manipulator (the distance between actuation points) as a small beam unto itself, and enforce continuity through the boundary conditions of each section. However, this method proves tedious and less insightful than its alternative, to introduce the field moments via a distributed moment term in the field equation (1a). Assuming that the actuators apply k point torques τ_i at locations σ_i, the distributed moment term will be

$$m(s) = \sum_{i=1}^{k} \tau_i \delta(s - \sigma_i), \qquad \sigma_1 < \cdots < \sigma_m = L \tag{5}$$

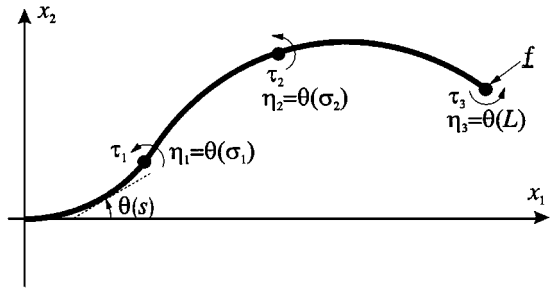

Fig. 3. Three-actuator continuum manipulator with applied end-effector force $\underline{f}$.

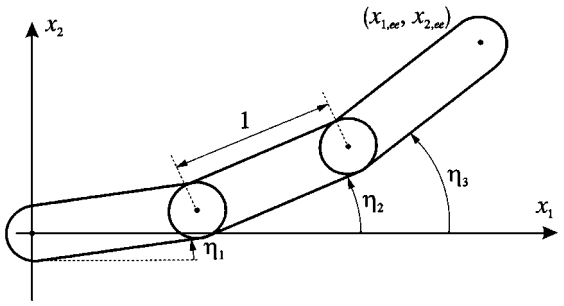

Fig. 4. Simple three-link manipulator.

where $\delta(s)$ is the standard Dirac delta function. It is important to realize that the moment applied to the end-effector appears as the kth moment in (5), despite the suggestion in (4c) that it is zero. Fig. 3 illustrates a three-section continuum backbone subject to an applied end-effector force $\underline{f}$.

III. Global Manipulability Ellipsoid (GME)

Consider the three-link manipulator of Fig. 4. The forward kinematics provide the mapping between the actuator joint angles, η_i, and $\underline{x}_{ee}$ as

$$\underline{x}_{ee} = \underline{g}(\underline{\eta}), \qquad \underline{\eta} = [\eta_1 \quad \eta_2 \quad \eta_3]. \tag{6}$$

If the joint angles have given angular velocities, then the velocity of the end-effector is linearly related to the velocities of the joints, so that

$$\dot{\underline{x}}_{ee} = J(\underline{\eta})\dot{\underline{\eta}}, \qquad J \triangleq \frac{\partial \underline{g}(\underline{\eta})}{\partial \underline{\eta}} \tag{7}$$

where J is the manipulator Jacobian. In the case of our example three-link robot, we find that

$$J = \begin{bmatrix} -s_{\eta_1} & -s_{\eta_2} & -s_{\eta_3} \\ c_{\eta_1} & c_{\eta_2} & c_{\eta_3} \end{bmatrix}. \tag{8}$$

The traditional manipulability ellipsoid answers the question, what is the set of all $\dot{\underline{x}}_{ee}$ such that $\dot{\underline{\eta}}$ has unit norm? That is,

$$\left\{ \dot{\underline{x}}_{ee} \colon \left\| \dot{\underline{\eta}} \right\| = \sqrt{\dot{\underline{\eta}}^T \dot{\underline{\eta}}} = 1 \right\}. \tag{9}$$

We will not repeat the explicit derivation of the manipulability ellipsoid (see [34]), but with the appropriate aid of singular value and eigenvalue decompositions, we note that the ellipsoid will have principal axes in the directions $\underline{v}_i$, with magnitudes $\sqrt{\lambda_i}$, where $\underline{v}_i$ and λ_i are the eigenvectors and eigenvalues of the symmetric product JJ^T. (We make the important remark that the robot pictured above is a remote-drive robot, as is the class of continuum robots under consideration here. These manipulators employ absolute joint angle measurements, whereas integrated or direct-drive robots use relative angle measurements and therefore a slightly different ellipsoid definition.)

A natural extension of the traditional manipulability measure to continuum robots utilizes a functional norm for the continuous angle velocity $\dot{\underline{\theta}}(s)$. We define the GME as

$$\text{GME} = \left\{ \dot{\underline{x}}(L) \colon \left\| \dot{\theta}(s) \right\| = 1 \right\} \tag{10}$$

where

$$\left\| \dot{\theta}(s) \right\|^2 = \int_0^L \dot{\theta}(s)^2 \, ds. \tag{11}$$

The set above is termed "global" because it employs the infinite dimensional functional norm of $\dot{\theta}$, accounting for all possible changes in the backbone angle, *even changes not physically achievable*, by the finite number of actuators exerting moments on the backbone. We first decompose the solution into an infinite sum of orthonormal modal basis functions

$$\theta(s) = \sum_{i=1}^{\infty} a_i \phi_i(s) = \underline{a}^T \underline{\phi}(s) \tag{12}$$

where the vectors $\underline{a}$ and $\underline{\phi}$ are infinitely long. The functions $\phi_i(s)$ can represent any orthonormal basis set defined over $[0, L]$, under the reasonable assumption that $\theta(s) \in L^2$. (For instance, in [10] we discuss the use of wavelet basis sets; normalized Legendre polynomials would also work well.) Orthonormality requires

$$a_i = \int_0^L \phi_i(s)\theta(s)\, ds, \qquad \int_0^L \phi_i(s)\phi_j(s)\, ds = \delta_{ij} \tag{13}$$

where δ_{ij} is the Kronecker delta. Given that $\underline{x}(L) = \int_0^L \underline{q}(\theta(s))\, ds$, use of the chain rule yields the time derivative of $\underline{x}(L)$

$$\dot{\underline{x}}(L) = \int_0^L \frac{\partial \underline{q}}{\partial \theta} \frac{\partial \theta}{\partial \underline{a}} \frac{\partial \underline{a}}{\partial t}\, ds = \left[\int_0^L T^T \underline{q}\, \underline{\phi}^T \, ds \right] \dot{\underline{a}} \triangleq J_m \dot{\underline{a}} \tag{14}$$

where the subscript m indicates the modal Jacobian. Obviously, the Jacobian defined above will have infinitely many columns and clearly does not lend itself to the direct computation of singular values and principal direction vectors as in [34]. However, close inspection of J_m

$$J_m = \begin{bmatrix} -\int s_\theta \phi_1 \, ds & -\int s_\theta \phi_2 \, ds & \cdots \\ \int c_\theta \phi_1 \, ds & \int c_\theta \phi_2 \, ds & \cdots \end{bmatrix} \tag{15}$$

reveals that each element is simply a coefficient in the spectral transformation of either s_θ or c_θ. In fact, let us define

$$p_i = \int_0^L \phi_i(s) \sin(\theta)\, ds \quad q_i = \int_0^L \phi_i(s) \cos(\theta)\, ds \tag{16}$$

and then note that the product $J_m J_m^T$ is

$$J_m J_m^T = \begin{bmatrix} \sum p_i^2 & -\sum p_i q_i \\ -\sum p_i q_i & \sum q_i^2 \end{bmatrix}. \tag{17}$$

Two properties of orthonormal spectral transformations come to our aid now, allowing simplification of the elements of $J_m J_m^T$

$$J_m J_m^T = \begin{bmatrix} \int_0^L {s_\theta}^2\, ds & -\int_0^L s_\theta c_\theta\, ds \\ -\int_0^L s_\theta c_\theta\, ds & \int_0^L {c_\theta}^2\, ds \end{bmatrix}. \quad (18)$$

The diagonals reflect the Parseval equality, and the off diagonals can be easily verified with use of (16) and the orthonormality property of (13).

As with the traditional manipulability ellipsoid, the GME will have principal direction vectors $\underline{v}_i$ with magnitudes $\sqrt{\lambda_i}$, where $\{\underline{v}_1, \underline{v}_2\}$ and $\{\lambda_1, \lambda_2\}$ are the eigenvectors and eigenvalues of $J_m J_m^T$. Interestingly, the precise choice of spectral decomposition chosen above does not really matter, as long as it adheres to the requirement of orthonormality. Note the intuitive similarity between (18) and the same quantity for the traditional three-link manipulator previously mentioned, where

$$JJ^T = \begin{bmatrix} \sum_{i=1}^{3} {s_{\theta_i}}^2 & -\sum_{i=1}^{3} c_{\theta_i} s_{\theta_i} \\ -\sum_{i=1}^{3} c_{\theta_i} s_{\theta_i} & \sum_{i=1}^{3} {c_{\theta_i}}^2 \end{bmatrix}. \quad (19)$$

Examples of the GME will appear shortly.

IV. Constrained Manipulability Ellipsoid (CME)

Essentially, the GME illustrates how the end-effector would move if an infinite number of actuators (or a distributed actuator) were specifying the shape of the backbone. In currently practical designs the function $\theta(s)$ is constrained to move only in certain directions dictated by the actuator positions and the physics acting on the backbone; that is, the actuators specify $\{\theta(\sigma_1) \cdots \theta(\sigma_k)\}$. This constraint is captured by a functional mapping from the actuator positions to the modal coefficients a_i

$$h\colon \{\theta(\sigma_1) \cdots \theta(\sigma_k)\} \rightarrow \{a_i\}. \quad (20)$$

If we define $\theta(\sigma_i) \triangleq \eta_i$, we can rewrite the mapping as

$$\underline{a} = \underline{h}(\underline{\eta}). \quad (21)$$

In general, $\underline{h}$ is a one-to-many mapping, as there can be an infinitely large set $\{a_i\}$. Because of this, the modal decomposition in the derivation of the GME required the property of orthonormality in order to arrive at a closed-form simplification of the product $J_m J_m^T$.

Consider, however, a (possibly nonorthogonal) set of basis functions ϕ_i for which $\theta(s)$ can be reconstructed either exactly, or to close precision, with a finite small number of coefficients a_i. In this case, the mapping $\underline{h}$ is finite to finite, or even one to one, permitting direct calculation of JJ^T. We have chosen to employ the finite–element method (FEM) to explore this possibility.

In its simplest form, a finite element procedure computes representative samples of a continuous function and interpolates between them to reconstruct that function. The representative

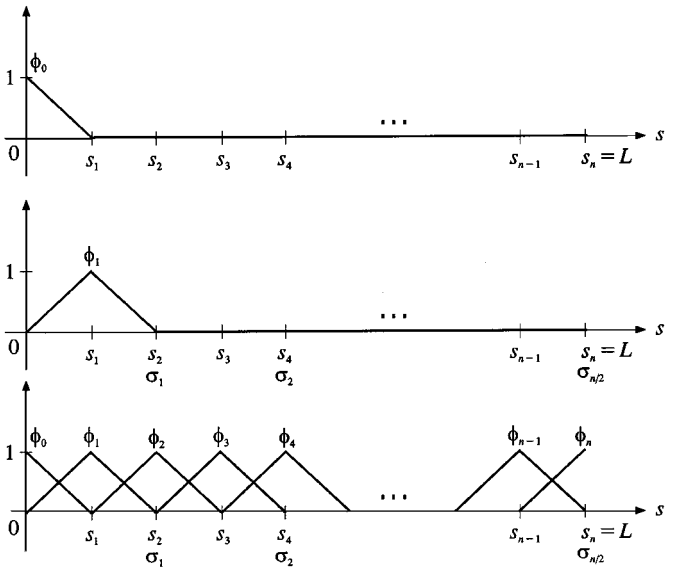

Fig. 5. The first two finite element interpolation functions, followed by all $n + 1$ functions superimposed.

samples can be thought of as the coefficients a_i, the interpolation functions as the modes $\phi_i(s)$, and the reconstructed function as $\theta(s) = \underline{a}^T \underline{\phi}(s)$. Intuitively, a good reconstruction will require at least as many samples as the number of actuators; in general, it will require more. In the absence of constraints or arguments to the contrary, the simple linear interpolation functions seen in Fig. 5 are overwhelmingly chosen in finite element work

$$\phi_i(s) = \begin{Bmatrix} \left(\dfrac{s - s_{i-1}}{s_i - s_{i-1}}\right), & s_{i-1} < s \le s_i \\ \left(\dfrac{s_{i+1} - s}{s_{i+1} - s_i}\right), & s_i < s \le s_{i+1} \\ 0, & \text{otherwise} \end{Bmatrix} \quad (22)$$

where $s_0 = 0$ and $s_n = L$. The locations s_i are termed nodes, and note we have specified that the cable termination locations σ_j must correspond to node locations s_{2j} in Fig. 5. (The exact ratio of nodes to actuator locations need not be 2 : 1 as in the figure; this is just for the sake of illustration.)

The Appendix uses the FEM to derive a relationship between the node displacements a_i and the applied node moments τ_i

$$K_m \underline{a} = \underline{\tau} + J_m^T \underline{f}. \quad (23)$$

Taking a time derivative of (23) yields

$$K \dot{\underline{a}} = \dot{\underline{\tau}} \quad (24)$$

with

$$K = K_m - K_t, \qquad K_t = \frac{\partial}{\partial \underline{a}} \left(J_m^T \underline{f}\right). \quad (25)$$

Matrix K_m is the material stiffness matrix, and K_t is the distributed force tangent matrix. Note K will be symmetric but deficient in rank by one dimension. Both vectors $\underline{a}$ and $\underline{\tau}$ have some specified and some unspecified elements. For each angular displacement a_i that is specified by an actuator, the corresponding moment τ_i is unspecified. Conversely, specified mo-

ments correspond to unspecified angles. Thus, we may subdivide relationship (24) so that

$$\begin{bmatrix} K_{11} & K_{12} \\ K_{21} & K_{22} \end{bmatrix} \begin{bmatrix} \underline{\dot{a}}_s \\ \underline{\dot{a}}_u \end{bmatrix} = \begin{bmatrix} \underline{\dot{\tau}}_u \\ \underline{\dot{\tau}}_s \end{bmatrix} \tag{26}$$

where subscripts s and u indicate specified and unspecified, respectively. With a little manipulation, the unspecified angular displacements can be determined in terms of the specified moments, so

$$\underline{\dot{a}}_u = K_{22}^{-1} \left(\underline{\dot{\tau}}_s - K_{21} \underline{\dot{a}}_s \right). \tag{27}$$

Since applied moments at backbone locations not co-located with actuators are zero, we have

$$\underline{\dot{a}}_u = -K_{22}^{-1} K_{21} \underline{\dot{a}}_s \tag{28}$$

and, remembering that $\underline{a}_s = \underline{\eta}$

$$\underline{\dot{a}} = \begin{bmatrix} \underline{\dot{a}}_s \\ \underline{\dot{a}}_u \end{bmatrix} = \begin{bmatrix} I_{k\times k} \\ -K_{22}^{-1} K_{21} \end{bmatrix} \underline{\dot{\eta}} \tag{29}$$

where $I_{k\times k}$ denotes the $k \times k$ identity matrix. Note that, as long as at least one angle is given somewhere along the backbone, K_{22} will be invertible. (It should be mentioned that, in the case of no applied end-effector load $\underline{f}$, the kinematics in (1a) yield a piecewise linear function for $\theta(s)$. This is a special case that the FEM can solve exactly. In this case, there is little point in making the dimension of $\underline{a}$ any larger than the number of actuators k, so (29) will be a pure identity, as explored in [12].)

Now we come to the definition of the CME

$$\text{CME} = \left\{ \underline{\dot{x}}(L) \colon \left\| \underline{\dot{\eta}} \right\| = 1 \right\}. \tag{30}$$

Augmenting the modal Jacobian in relationship (14) with (29) gives

$$\underline{\dot{x}}(L) = J_a \underline{\dot{\eta}}, \qquad J_a = J_m \begin{bmatrix} I_{k\times k} \\ -K_{22}^{-1} K_{21} \end{bmatrix} \tag{31}$$

where J_a is the actuator Jacobian. Consequently, the CME will have principal axis vectors $\underline{v}_i$ with magnitudes $\sqrt{\lambda_i}$, where $\{\underline{v}_1, \underline{v}_2\}$ and $\{\lambda_1, \lambda_2\}$ are the eigenvectors and eigenvalues of $J_a J_a^T$.

Consider Fig. 6, which illustrates a one-section manipulator with no applied end-effector force. While the CME reflects the obvious fact that a single-actuator manipulator is always singular with respect to a two-dimensional positioning requirement, the GME illustrates that the device as a whole is not in a singular configuration. This is an important distinction, as it highlights two different types of singularities that continuum manipulators can experience: actuator singularities, where the robot cannot move in a given direction for lack of actuation, and configuration singularities, where the robot cannot move in a given direction under any circumstances. Fig. 7 illustrates the GME and CME for a given configuration, giving the robot successively more actuators. Notice that, as the number of actuators increases, the dimensions of the CME approach those of the GME.

(The parameters used for generating the examples are $EI = L = 1$. There is no loss of generality because simulated quantities relate to actual quantities via $s = s_a/L_a$, $\underline{x} = \underline{x}_a/L_a$, $\underline{f} = \underline{f}_a L_a^2/EI_a$, $m = m_a L_a/EI_a$, where a subscripts indicate actual physical measurements.)

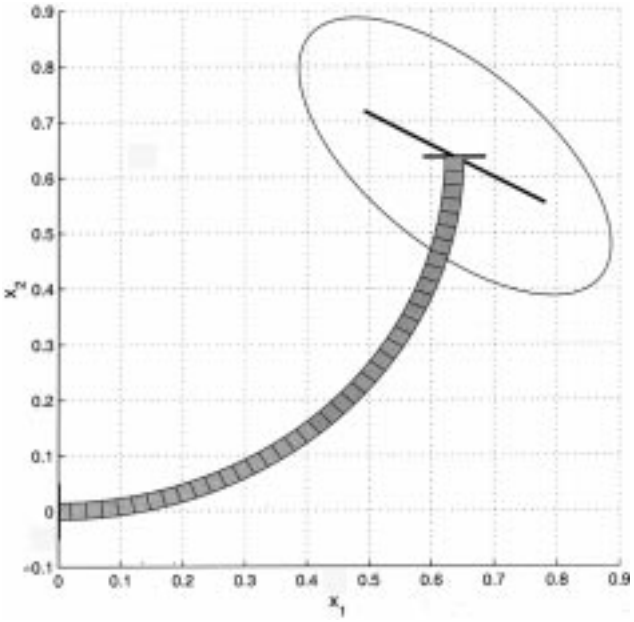

Fig. 6. For a one-section manipulator, the CME indicates a singular configuration (bold line) while the GME does not (thin line).

V. Global Force Ellipsoid (GFE)

In a rigid-link manipulator, the Jacobian also defines a simple force–torque relationship between the end-effector and the actuators

$$\underline{\tau} + J^T \underline{f} = \underline{0}. \tag{32}$$

(In this paper, we have spoken of forces as the generalized forces exerted *on* the end-effector, and of torques as the generalized forces exerted *by* the actuators.) The traditional force ellipsoid describes all the end-effector forces that a robot can produce given actuator torques of unit norm

$$\left\{ \underline{f} \colon \|\underline{\tau}\| = 1 \right\}. \tag{33}$$

A simple calculation reveals that the force ellipsoid has principal axis vectors $\underline{v}_i$ with magnitudes $1/\sqrt{\lambda_i}$, where $\underline{v}_i$ and λ_i are the eigenvectors and eigenvalues of JJ^T. Thus, the force ellipsoid is perpendicular to the manipulability ellipsoid, indicating that the directions in which the robot can exert the greatest forces are also the directions in which it is least sensitive to changes in the actuator displacements.

We approach the derivation of the force–torque relationship for a continuum manipulator in much the same way as for traditional manipulators; however, there are a number of differences in interpretation. For one, unlike with rigid-link designs, the torques felt at the actuators must necessarily reflect the potential energy of the backbone (i.e., its strain or deformation energy). In other words, nonzero moments are required simply to hold the manipulator in a given pose, even in the absence of gravity or applied end-effector loads. Consequently, we must speak of how a differential change in applied moments (in the

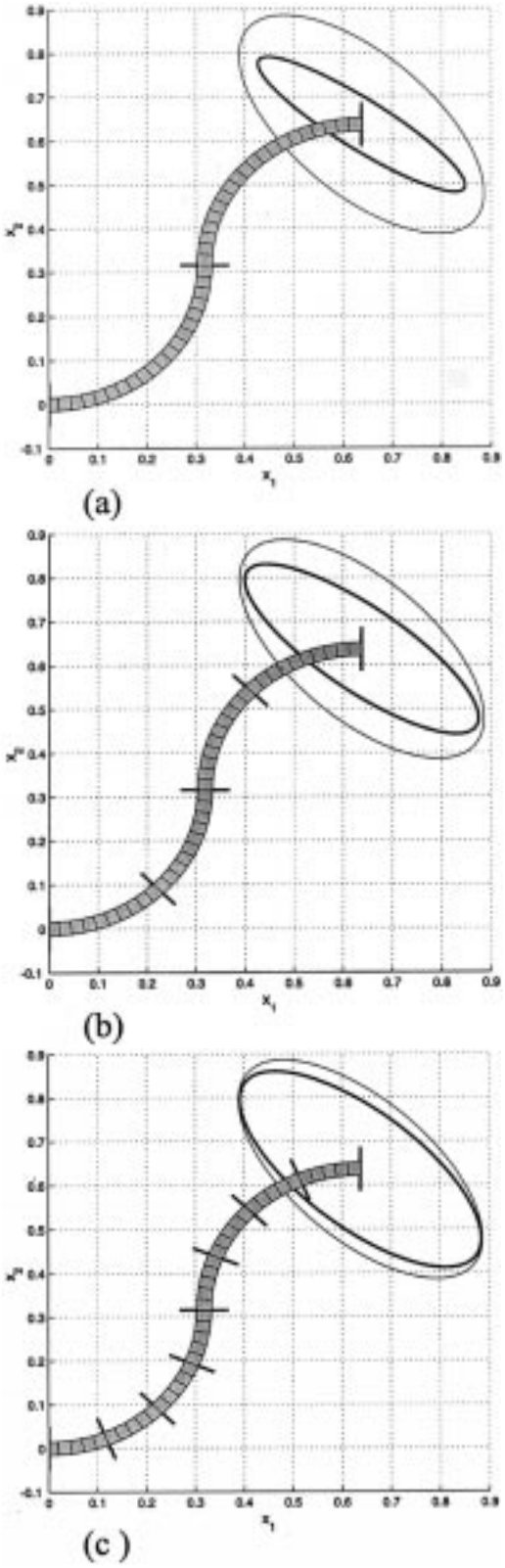

Fig. 7. For a given configuration, adding actuators "fills out" the CME (bold line) so that it approaches the dimension of the GME (thin line).

applied moment density function, actually) results in a change in potential energy.

We begin by introducing a simple two-step thought experiment. In step 1, we allow the robot to assume a pose with a strain energy of P_a, distributed moment $m_a(s)$, and no applied load. Thus, the principle of virtual work dictates

$$\delta P_a = \delta W_a \Rightarrow \int_0^L EI\theta_a'\delta\theta_a'\,ds = \int_0^L m_a\delta\theta_a\,ds. \quad (34)$$

In step 2, we then change the applied moment density to $m_b(s)$, but simultaneously keep the end-effector at the same location by exerting force $\underline{f}$ on the end-effector. Consequently,

$$\delta P_b = \delta W_{b1} + \delta W_{b2} \Rightarrow \int_0^L EI\theta_b'\delta\theta_b'ds = \int_0^L m_b\delta\theta_b ds + \underline{f}^T\delta\underline{x}_b(L). \quad (35)$$

Since $\delta\theta_a(s)$ and $\delta\theta_b(s)$ have the same geometric boundary conditions ($\delta\theta_a(0) = \delta\theta_b(0) = 0$), but are otherwise arbitrary, we may equalize them without loss of generality, so $\delta\theta_a = \delta\theta_b = \delta\theta$. Then, subtracting (34) from (35) and integrating the left-hand side by parts with reference to (4a) and (4c) gives

$$\int_0^L EI\Delta\theta''\delta\theta\,ds = \int_0^L \Delta m\delta\theta\,ds + \underline{f}^T\delta\underline{x}_b(L) \quad (36)$$

where $\Delta\theta = \theta_a - \theta_b$ and $\Delta m = m_a - m_b$. (Distribution of integrals and derivatives through variations is a standard procedure in variational calculus and appears frequently in works such as [24].) We may substitute for the second term of the right-hand side above

$$\delta\underline{x}_b(L) = \int_0^L T^T\underline{q}_b\delta\theta\,ds. \quad (37)$$

Then, recalling that $\delta\theta$ is arbitrary, the fundamental theorem of variational calculus gives

$$EI\Delta\theta'' = \Delta m + \underline{f}^T T^T\underline{q}_b. \quad (38)$$

At this point, it is immediately evident that a force contour corresponding to a constant change in distributed moment (those $\underline{f}$ corresponding to $\|\Delta m\| = 1$) will not be elliptical in general. This is because not all work applied to (or extracted from) the backbone produces work at the end-effector. Some of the applied work increases (or decreases) the backbone strain energy. If, however, we make the assumption that, for relatively small applied forces, the backbone configuration change is negligibly small, i.e., $EI\Delta\theta'' \approx 0$, then we may rewrite (38) as

$$\Delta m + \underline{f}^T T^T\underline{q} = 0. \quad (39)$$

(Where it is unambiguous, we will drop the subscript b.) The accuracy of this assumption has been borne out with experience; nevertheless, it relegates (39) to an approximation, and further illustrates the differences between continuum robots and traditional robots.

Now a quadratic relationship can be found, which we will call the GFE

$$\text{GFE} = \left\{\underline{f}\colon \|\Delta m\| = 1\right\}. \quad (40)$$

Employing relation (39), the GFE requires

$$\|\Delta m\|^2 = \int_0^L (\Delta m)^2\,ds = \underline{f}^T\left[T^T\int_0^L \underline{q}\,\underline{q}^T\,dsT\right]\underline{f} = 1. \quad (41)$$

This reads in expanded form as

$$\underline{f}^T \begin{bmatrix} \int s_\theta^2\, ds & -\int c_\theta s_\theta\, ds \\ -\int c_\theta s_\theta\, ds & \int c_\theta^2\, ds \end{bmatrix} \underline{f} = 1 \tag{42}$$

which can be seen by reference to (18) as $\underline{f}^T J_m J_m^T \underline{f} = 1$. As a result, the GFE will have principal axis vectors of $\{\underline{v}_1, \underline{v}_2\}$ with magnitudes $\{1/\sqrt{\lambda_1}, 1/\sqrt{\lambda_2}\}$ where $\underline{v}_i$ and λ_i are the eigenvectors and eigenvalues of $J_m J_m^T$. As with the traditional force and manipulability ellipsoids, the principal axes of the GFE have magnitudes in inverse proportion to those of the GME, while still pointing in the same direction.

VI. Constrained Force Ellipsoid (CFE)

As we noted in the derivation of the CME, the moment density function cannot assume arbitrary values. It is constrained because the actuators may only act at distinct physical locations. As in the Appendix, we may write the moment density as

$$m(s) = \underline{\delta}(s)^T \underline{\tau} \tag{43}$$

where

$$\underline{\delta}(s) = \begin{bmatrix} \delta(s-s_0) & \delta(s-s_1) & \cdots & \delta(s-s_n) \end{bmatrix}^T. \tag{44}$$

Again, we formulate the backbone angle as a weighted sum of interpolation basis functions, $\theta(s) = \underline{a}^T \underline{\phi}(s)$. Taking the first variation of the end-effector work gives

$$\begin{aligned} \delta W_{b2} &= \underline{f} \cdot \delta \underline{x}(L) \\ &= \underline{f} \cdot \int_0^L \delta \underline{q}\, ds \\ &= \underline{f}^T \int_0^L T^T \underline{q} \delta\theta\, ds \\ &= \underline{f}^T \int_0^L T^T \underline{q}\, \underline{\phi}^T \delta \underline{a}\, ds \\ &= \underline{f}^T \left[\int_0^L T^T \underline{q}\, \underline{\phi}^T ds \right] \frac{\partial \underline{a}}{\partial \underline{\eta}} \delta \underline{\eta} \\ &= \underline{f}^T J_m \begin{bmatrix} I_{m\times m} \\ -K_{22}^{-1} K_{21} \end{bmatrix} \delta \underline{\eta} \\ &= \underline{f}^T J_a \delta \underline{\eta}. \end{aligned} \tag{45}$$

With reference to (31), the first variation of the actuator work yields

$$\begin{aligned} \delta W_{b1} &= \int_0^L \Delta m \delta\theta\, ds \\ &= \left[\int_0^L \Delta m \underline{\phi}^T ds \right] \frac{\partial \underline{a}}{\partial \underline{\eta}} \delta \underline{\eta} \\ &= \left[\int_0^L (\Delta \underline{\tau})^T \underline{\delta}(s) \underline{\phi}(s)^T ds \right] \begin{bmatrix} I_{m\times m} \\ -K_{22}^{-1} K_{21} \end{bmatrix} \delta \underline{\eta} \\ &= \Delta \underline{\tau}^T \left[\int_0^L \underline{\delta}(s) \underline{\phi}(s)^T ds \right] \begin{bmatrix} I_{m\times m} \\ -K_{22}^{-1} K_{21} \end{bmatrix} \delta \underline{\eta} \\ &= \Delta \underline{\tau}_s^T \delta \underline{\eta}. \end{aligned} \tag{46}$$

To complete the last equality above, note that $\int_0^L \underline{\delta}(s) \underline{\phi}(s)^T ds = I$. Also, applied moments at locations with no actuator attachments must be zero. Thus, the only nonzero elements of $\underline{\tau}$ are the specified moments $\underline{\tau}_s$ that, by definition, correspond to the identity rows of matrix $\partial \underline{a}/\partial \underline{\eta}$.

Invoking the assumption that the net change in backbone strain energy is negligible, the principle of virtual work then equates $\delta W_{b1} + \delta W_{b1} = 0$, giving

$$\Delta \underline{\tau}_s^T + \underline{f}^T J_a = \underline{0} \tag{47}$$

where we have eliminated $\delta \underline{\eta}$ from both sides because its value is arbitrary. Intuitively, this result parallels that of a rigid-link manipulator. If we define the CFE as

$$\text{CFE} = \left\{ \underline{f} \colon \|\Delta \underline{\tau}_s\| = 1 \right\} \tag{48}$$

then it will have principal axis vectors $\{\underline{v}_1, \underline{v}_2\}$ with magnitudes $\{1/\sqrt{\lambda_1}, 1/\sqrt{\lambda_2}\}$ where $\underline{v}_i$ and λ_i are the eigenvectors and eigenvalues of $J_a J_a^T$.

As expected, a manipulator with numerous actuators will have a CFE more closely approximating the GFE than one with few actuators. Fig. 8 illustrates this for two manipulators in the same configuration, one with eight actuators and one with only four. However, there is a subtle interpretational difference from the force ellipsoids of traditional robots. Fig. 8 would seem to counterintuitively suggest that continuum robots with few actuators can apply, or resist, forces of larger magnitude than robots with many actuators, for a given configuration. While for a rigid-link robot, this conclusion is sound, such a conclusion may not apply in the case of a continuum robot. Fig. 8 simply illustrates the relative force magnitudes that will generate unit norm changes in the applied moments. Clearly the robot of Fig. 6 cannot resist forces of infinite magnitude perpendicular to its CME because it is not in a *configuration* singularity, only an *actuation* singularity.

VII. Compliance Ellipsoid (CE)

Perhaps one of the greatest assets of a continuum manipulator is its inherent passive compliance. Passive compliance, i.e., compliance built into a mechanism via purely mechanical means, can often eliminate the need for complex and expensive force/torque sensors and feedback systems. Passive compliance is suggested in [18] as a practical and straightforward means to increase the safety margin of human–robot interaction without relying on third-person vision systems or impractical sensor skins, and without sacrificing the precision or utility of a manipulator. Additionally, compliance will almost certainly be a necessary ingredient in the successful formulation of whole arm grasping algorithms for hyperredundant robots.

The CE provides the critical first step in evaluating and effectively using a compliant system. We are interested here in the natural system compliance, the ability of the manipulator to comply while the actuators hold fixed positions. There are several possible definitions of CEs. We choose one based on variational concepts

$$CE = \left\{ \delta \underline{x}(L) \colon \left\| \delta \underline{f} \right\| = 1 \right\}. \tag{49}$$

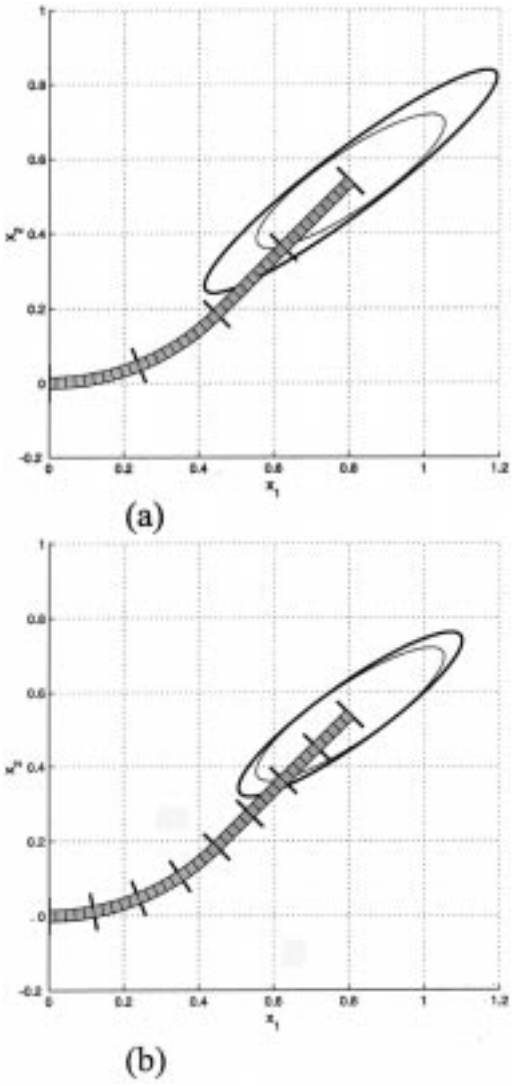

Fig. 8. An illustration of the CFE (bold line) and the GFE (thin line) for two manipulators in the same configuration but with differing numbers of actuators.

Essentially, we want to know where the end-effector will move under the influence of external unit forces.

Logically, the key to understanding the relationship between a small applied force and the induced incremental change in end-effector position is found in the compliance matrix $\partial \underline{x}(L)/\partial \underline{f}$ that relates the two. The finite–element formulation comes to our aid again. Recall that $\underline{x}(L) = \int_0^L \underline{q}(\theta(s))\, ds$ and $\theta(s) = \underline{a}^T \underline{\phi}(s)$, so

$$\frac{\partial \underline{x}(L)}{\partial \underline{f}} = \int_0^L \left(\frac{\partial \underline{q}}{\partial \underline{a}}\right) ds \frac{\partial \underline{a}}{\partial \underline{f}} = J_m \frac{\partial \underline{a}}{\partial \underline{f}}. \tag{50}$$

We may differentiate (23) with respect to $\underline{f}$, remembering to account for implied dependence of the modal coefficients on $\underline{f}$ with the chain rule

$$\left[K_m - \frac{\partial \left(J_m^T \underline{f}\right)}{\partial \underline{a}}\right] \frac{\partial \underline{a}}{\partial \underline{f}} = \frac{\partial \underline{\tau}}{\partial \underline{f}} + J_m^T. \tag{51}$$

We previously assigned the sum

$$\left[K_m - \frac{\partial}{\partial \underline{a}} \left(J_m^T \underline{f}\right)\right] \triangleq K$$

and noted that it is always symmetric and invertible. Again, it is convenient to subdivide the expression above into two sets of equations: one set for the specified quantities (node displacements or moments), and one set for the unspecified quantities. Doing so yields

$$\begin{bmatrix} K_{11} & K_{12} \\ K_{21} & K_{22} \end{bmatrix} \begin{bmatrix} 0 \\ \partial \underline{a}_u / \partial \underline{f} \end{bmatrix} = \begin{bmatrix} \partial \underline{\tau}_u / \partial \underline{f} \\ 0 \end{bmatrix} + J_m^T \tag{52}$$

where we note that the specified node displacements correspond to actuator angles that are not changing with respect to end-effector force, and the specified node moments are all zero. Thus, we arrive at a solution for the desired quantity

$$\frac{\partial \underline{a}}{\partial \underline{f}} = \begin{bmatrix} 0 \\ \partial \underline{a}_u / \partial \underline{f} \end{bmatrix} = \begin{bmatrix} 0 & 0 \\ 0 & K_{22}^{-1} \end{bmatrix} J_m^T. \tag{53}$$

We may then rewrite (50) in the final desired form

$$\frac{\partial \underline{x}(L)}{\partial \underline{f}} = J_m \begin{bmatrix} 0 & 0 \\ 0 & K_{22}^{-1} \end{bmatrix} J_m^T \tag{54}$$

a 2×2 symmetric compliance matrix. Intuitively, this is the exact analog of the traditional compliance matrix, a product of manipulator Jacobians weighted by an inverse stiffness matrix. In this instance, the stiffness inverse is semidefinite, effectively canceling out columns of the modal Jacobian that correspond to fixed (and therefore incompliant) actuator nodes.

The CE will have principal axis vectors $\{\underline{v}_1, \underline{v}_2\}$ with magnitudes $\{\sqrt{\lambda_1}, \sqrt{\lambda_2}\}$ where $\underline{v}_i$ and λ_i are the eigenvectors and eigenvalues of the compliance matrix (54).

Figs. 9 and 10 illustrate the nature of the compliance ellipsoid. In each figure, a two-actuator robot starts in the same no-load configuration, and then experiences the application of end-effector forces of 10 and then 20 units. When applied in the negative x_2 direction (Fig. 9), the same forces produce a much greater end-effector displacement than when applied in the negative x_1 direction (Fig. 10). Although these forces, and the associated displacements, can hardly be considered incremental (as per the definition of the CE), the ellipsoid gives excellent insight into the relative response of the backbone in each case.

VIII. Conclusions

To summarize, the purpose of this paper has been to explore the manipulability, force, and compliance characteristics of an emerging class of hyperredundant robots called continuum manipulators, using ellipsoid analysis. We formulated five types of ellipsoids, with the assistance of FEMs in some cases, and produced examples of each. The results bring us one step closer to the goal of deploying continuum robots for tasks for which they are well suited: those requiring the delicacy of passive compliance, whole-arm manipulation, or other tentacle or trunklike behaviors.

Needless to say, much remains to be done. The specifics of how a tentacle robot achieves a whole-arm task remain unclear (what kinds of motions can be achieved, what sensors are required, etc.). Also, the modeling and analysis work must progress into the three-dimensional regime, a leap much less intuitive and more difficult than the transition from two–dimensional to three-dimensional rigid-link robots. Current work

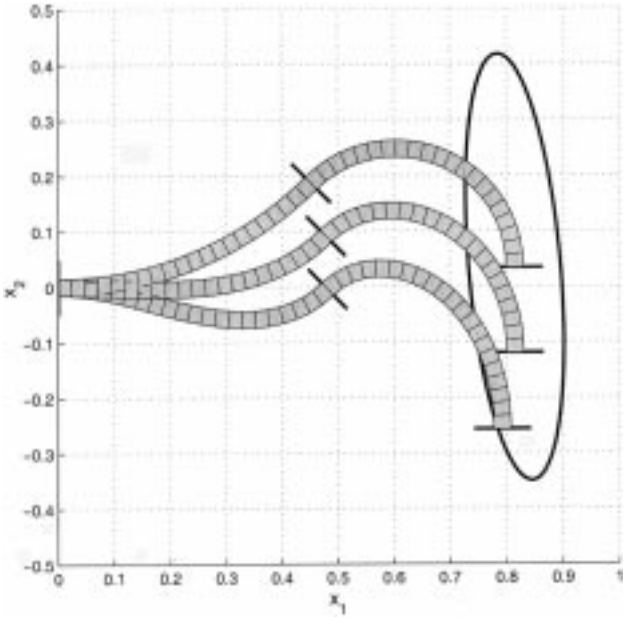

Fig. 9. A compliance ellipsoid indicates that the robot is more compliant to vertical forces on the end-effector than horizontal forces.

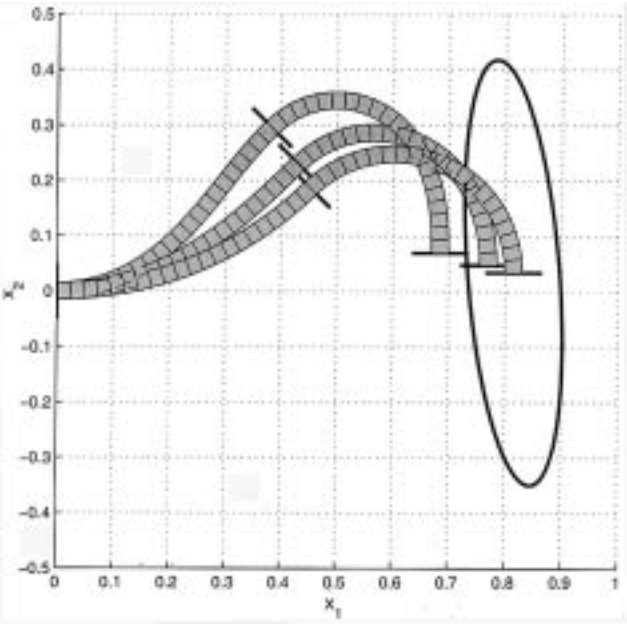

Fig. 10. Forces of the same magnitude as the previous figure encounter relatively less compliance in the horizontal direction.

is focusing on both of these objectives, in addition to ongoing mechanical and design improvements.

APPENDIX

The FEM begins by dividing the domain of the unknown continuous function (or functions) into a set of n sections, called elements, joined by $n+1$ nodes. Each node is assigned at least one primary displacement variable (positions and/or angles) and an associated dual variable (forces and/or moments). The unknown function is then synthesized by interpolating between the primary variables, i.e., adding up $n+1$ local interpolation functions whose amplitudes are the values of the corresponding primary variables. We will not delve into the mathematical justification for the FEM or the rules for determining what interpolation functions to use in this paper (see, e.g., [9] for more details).

In our case, we wish to synthesize the unknown function $\theta(s)$. Referring back to (1), its governing equation is

$$EI\theta'' + \underline{q}^T T \underline{f} + m = 0 \tag{55}$$

which is a nonlinear function θ. The moment density function provides the mechanism whereby nodal moments enter the equation

$$m(s) = \sum_{i=0}^{n} \tau_i \delta(s - s_i) = \underline{\tau}^T \underline{\delta}(s), \qquad 0 = s_0 < s_1 < \cdots < s_n = L \tag{56}$$

where the s_i are the locations of the nodes. Strictly speaking, since the robot has only $k < n$ actuators, (55) should use the moment density function of (5), rather than (56). However, we will remedy this shortly by specifying that the remaining $n+1-k$ moments in (56) are zero. Note that the τ_i are the dual variables, and as described throughout this paper, we now synthesize $\theta(s)$ as a weighted sum of interpolation functions $\theta(s) = \underline{a}^T \underline{\phi}(s)$, where the a_i are the primary variables. (An important characteristic of interpolation functions is that $\phi_i(s_i) = 1$ and $\phi_i(s_{j \neq i}) = 0$, so the a_i can be thought of as samples of the function $\theta(s)$, though they will actually only be approximations. Refer back to Fig. 5.)

The so-called weak form, or variational form, of (55) gives

$$\int_0^L w(s) \left(EI\theta'' + \underline{q}^T T \underline{f} + \underline{\tau}^T \underline{\delta} \right) \, ds = 0 \tag{57}$$

with $w(s)$ an arbitrary weighting function subject to the same boundary conditions as $\theta(s)$. Integrating the left-most term by parts gives

$$\int_0^L \left(EIw'\theta' \right) \, ds = \int_0^L \left(w \underline{\tau}^T \underline{\delta} + w \underline{q}^T T \underline{f} \right) \, ds \tag{58}$$

where we have used $w(0) = 0$ and (4c) to simplify. Because $w(s)$ is arbitrary, we may synthesize it as a weighted sum of the interpolation functions with coefficients b_i

$$w(s) = \underline{b}^T \underline{\phi}(s) \tag{59}$$

without loss of generality. Note that now the b_i are arbitrary. Substituting the weighted-sum versions of $w(s)$ and $\theta(s)$ back into (58)

$$\underline{b}^T \left[\left(\int_0^L EI \underline{\phi}' \, \underline{\phi}'^T \, ds \right) \underline{a} \right] = \underline{b}^T \left[\left(\int_0^L \underline{\phi} \, \underline{\delta}^T \, ds \right) \underline{\tau} + \int_0^L \underline{\phi} \, \underline{q}^T T \underline{f} \, ds \right] \tag{60}$$

allowing cancellation of the arbitrary $\underline{b}$ on each side. After one definition and two simplifications

$$\int_0^L EI\underline{\phi}'\,\underline{\phi}'^T\,ds \triangleq K_m$$
$$\int_0^L \underline{\phi}\,\underline{q}^T T\underline{f}\,ds = J_m^T\underline{f}$$
$$\int_0^L \underline{\phi}\,\underline{\delta}^T\,ds = I_{(n+1)\times(n+1)} \tag{61}$$

we may rewrite (60) as

$$K_m\underline{a} = \underline{\tau} + J_m\underline{f}. \tag{62}$$

Expression (62) is the essential relation between the primary and dual variables. In this problem, as is typical in finite–element analysis, some elements of $\underline{a}$ are specified *a priori* and some are not. Specified displacements, such as the initial angle ($a_0 = 0$), and perhaps intermediate angles held by the actuators to certain values, correspond with unknown moments ($\tau_0 = ?$). Similarly, nodes with specified moment application (e.g., nodes with no actuation, $\tau_j = 0$) must correspond with unknown displacements ($a_j = ?$). In any case, there are always just enough specified quantities to solve for both types of unknowns in (62).

Interestingly, manipulation of the time-differentiated version of (62), used in the derivation of the CME, provides exactly the right mechanism for solving (62). Except when $\underline{f} = \underline{0}$, (62) is nonlinear in $\underline{a}$ because

$$\underline{q} = \begin{bmatrix} c_\theta \\ s_\theta \end{bmatrix} = \begin{bmatrix} \cos\left(\underline{a}^T\underline{\phi}(s)\right) \\ \sin\left(\underline{a}^T\underline{\phi}(s)\right) \end{bmatrix}. \tag{63}$$

Consequently, an iterative solution algorithm based on (26) eliminates the need to solve a nonlinear boundary value equation with field constraints. This procedure is analogous to using the manipulator Jacobian to iteratively solve inverse kinematics problems. It exhibits fast convergence and was employed to create all of the simulation examples throughout this paper.

REFERENCES

[1] V. C. Anderson and R. C. Horn, "Tensor arm manipulator design," ASME, paper 67-DE-57, 1967.

[2] H. Asada, "A geometric representation of manipulator dynamics and its application to arm design," *ASME J. Dynam. Syst., Meas. Control*, vol. 105, pp. 131–142, 1983.

[3] P. Chiacchio, S. Chiaverini, L. Sciavicco, and B. Siciliano, "Global task space manipulability ellipsoids for multiple armed systems," *IEEE Trans. Robot. Automat.*, vol. 7, pp. 678–685, Oct. 1991.

[4] ——, "Task space dynamic analysis of multiarm system configurations," *Int. J. Robot. Res.*, vol. 10, no. 6, pp. 708–715, 1991.

[5] G. S. Chirikjian and J. W. Burdick, "Kinematically optimal hyperredundant manipulator configurations," *IEEE Trans. Robot. Automat.*, vol. 11, pp. 794–780, Dec. 1995.

[6] G. S. Chirikjian, "Theory and applications of hyperredundant robotic manipulators," Ph.D. dissertation, Dept. Appl. Mech., Calif. Inst. Technol., Pasadena, June 1992.

[7] ——, "Hyper-redundant manipulator dynamics: A continuum approximation," *Adv. Robot.*, vol. 9, no. 3, pp. 217–243, 1995.

[8] R. Cieslak and A. Morecki, "Elephant trunk type elastic manipulator—A tool for bulk and liquid materials transportation," *Robotica*, vol. 17, pp. 11–16, 1999.

[9] J. G. Eisley, *Mechanics of Elastic Structures*. Englewood Cliffs, NJ: Prentice-Hall, 1989.

[10] I. Gravagne and I. D. Walker, "Kinematic transformations for remotely-actuated planar continuum robots," in *Proc. IEEE Int. Conf. Robotics and Automation (ICRA)*, San Francisco, CA, May 2000, pp. 19–26.

[11] ——, "On the kinematics of remotely-actuated continuum robots," in *Proc. IEEE Int. Conf. Robotics and Automation (ICRA)*, San Francisco, CA, May 2000, pp. 2544–2550.

[12] ——, "Manipulability and force ellipsoids for continuum robot manipulators," in *Proc. IEEE/RSJ Int. Conf. Intelligent Robots and Systems (IROS)*, Maui, HI, Oct. 2001, pp. 304–311.

[13] Grey Pilgrim Company, Rockville, MD.. [Online]. Available: http://www.greypilgrim.com

[14] M. Hannan and I. D. Walker, "Novel kinematics for continuum robots," in *Proc. 7th Int. Symp. Advances in Robot Kinematics*, Piran, Slovenia, June 2000, pp. 227–238.

[15] ——, "Analysis and initial experiments for a novel elephant's trunk robot," in *Proc. Int. Conf. Intelligent Robots and Systems (IROS)*, Takamatsu, Japan, Nov. 2000, pp. 330–337.

[16] S. Hirose, *Biologically Inspired Robots*. London, U.K.: Oxford Univ. Press, 1993.

[17] S. Lee, "Dual redundant arm configuration optimization with task-oriented dual arm manipulability," *IEEE Trans. Robot. Automat.*, vol. 5, pp. 78–97, Jan. 1989.

[18] H. Lim and K. Tanie, "Human safety mechanisms of human-friendly robots: Passive viscoelastic trunk and passively movable base," *Int. J. Robot. Res.*, vol. 19, no. 4, pp. 307–335, Apr. 2000.

[19] E. H. Love, *A Treatise on the Mathematical Theory of Elasticity*. New York: Dover , 1944.

[20] S. Ma and M. Watanabe, "Minimum-time control of coupled tendon-driven manipulators," *Adv. Robot.*, vol. 15, no. 4, pp. 391–408, 2001.

[21] H. Mochiyama and H. Kobayashi, "The shape Jacobian of a manipulator with hyper degrees of freedom," in *Proc. 1999 IEEE Int. Conf. Robotics and Automation (ICRA)*, Detroit, MI, May 1999, pp. 2837–2842.

[22] ——, "Shape correspondence between a spatial curve and a manipulator with hyper degrees of freedom," in *Proc. 1998 IEEE/RSJ Int. Conf. Intelligent Robots and Systems (IROS)*, Victoria, B.C., Canada, Oct. 1998, pp. 161–166.

[23] F. C. Park and R. W. Brockett, "Kinematic dexterity of robotic mechanism," *Int. J. Robot. Res.*, vol. 14, no. 1, pp. 1–15, Feb. 1994.

[24] C. D. Rahn, *Mechatronic Control of Distributed Vibration and Noise*. Berlin, Germany: Springer-Verlag, 2001.

[25] G. Robinson and J. B. C. Davies, "Continuum robots—A state of the art," in *Proc. IEEE Int. Conf. Robotics and Automation*, Detroit, MI, May 1999, pp. 2849–2854.

[26] J. C. Simo, N. Tarnow, and M. Doblare, "Non-linear dynamics of three-dimensional rods: Exact energy and momentum conserving algorithms," *Int. J. Numer. Methods Eng.*, vol. 38, pp. 1431–1473, 1995.

[27] J. C. Simo and L. Vu-Quoc, "On the dynamics of flexible beams under large overall motions—The plane case," *J. Appl. Mech.*, vol. 53, pp. 849–863, Dec. 1986.

[28] K. Suzumori, S. Iikura, and H. Tanaka, "Applying a flexible microactuator to robotics mechanics," *IEEE Control Syst. Mag.*, vol. 12, pp. 21–26, Feb. 1992.

[29] M. W. Spong and M. Vidyasagar, *Robot Dynamics and Control*. New York: Wiley, 1989.

[30] H. Tsukagoshi, A. Kitagawa, and M. Segawa, "Active hose: An artificial elephant's nose with maneuverability for rescue operation," in *Proc. IEEE Int. Conf. Robotics and Automation (ICRA)*, Seoul, Korea, May 2001, pp. 2454–2459.

[31] I. D. Walker and M. W. Hannan, "A novel elephant's trunk robot," in *Proc. IEEE/ASME Int. Conf. Advanced Intelligent Mechatronics*, Atlanta, GA, Sept. 1999, pp. 410–415.

[32] I. D. Walker, "Impact configurations and measures for kinematically redundant and multiple armed robot systems," *IEEE Trans. Robot. Automat.*, vol. 10, pp. 670–682, Oct. 1994.

[33] J. F. Wilson and J. M. Snyder, "The elastica with end-load flip-over," *ASME J. Appl. Mech.*, vol. 55, no. 4, pp. 845–848, Dec. 1988.

[34] T. Yoshikawa, "Manipulability and redundancy control of redundant mechanisms," in *Proc. IEEE Int. Conf. Robotics and Automation (ICRA)*, 1985, pp. 1004–1009.

Ian A. Gravagne received the B.S. degree in electrical engineering in 1997 from Rice University, Houston, TX, and the M.S. and Ph.D. degrees in 1999 and 2002, respectively, from Clemson University, Clemson, SC.

He will join the the Department of Engineering, Baylor University, Waco, TX, in August, 2002. His research interests include redundant and hyperredundant mechanisms, mechanics and dynamics for highly flexible systems, optimization theory, and real-time operating systems.

Ian D. Walker (S'84–M'85–SM'02) received the B.Sc. degree in mathematics from the University of Hull, Hull, U.K., and the M.S. and Ph.D. degrees in electrical engineering from the University of Texas at Austin, in 1983, 1985, and 1989, respectively.

From 1989 to 1997, he was with the Department of Electrical and Computer Engineering, Rice University, Houston, TX, where he held the positions of Assistant Professor and Associate Professor. Since 1997, he has been with the Department of Electrical and Computer Engineering, Clemson University, Clemson, SC, where he currently is a Professor. His research interests are in robotics, particularly kinematically redundant robots, robot reliability and fault detection, and biologically inspired robots.

Dr. Walker is a member of Sigma Xi, Beta Alpha Phi, Eta Kappa Nu, Phi Kappa Phi, and Tau Beta Pi.